Supplementary Material (SM)

A: SLTORC Governing Equations in Lagrangian Coordinates

SLTORC solves the governing reacting flow equations in Lagrangian coordinates. Lagrangian coordinates have been used in previous studies to eliminate numerical difficulties arising from the non-linear advective term in the energy and species equations when expressed in Eulerian coordinates [1]. The governing equations for mass, energy, and species conservation expressed in Lagrangian coordinates are listed as Eqns. (1)-(3), respectively. Table S1 provides a description of the nomenclature chosen for variables in these equations.

Table S1. Variable nomenclature for governing SLTORC equations in Lagrangian coordinates.

t	Time	c_p	Species heat at constant pressure
r	Spatial coordinate	$\dot{m}$	Mass flux out of the system
ψ	Lagrangian coordinate	λ	Thermal conductivity
ρ	Density	A	Surface area
V	Volume	$c_{p,k}$	Species heat of species k
T	Temperature	D_k	Diffusion coefficient of species k
Y_k	Mass fraction of species k	$\dot{\omega}_k$	Volumetric production rate of species k
M	Total mass of the system	$\Delta h^0_{f,k}$	Standard enthalpy of formation of species k

Mass Conservation

$$\rho \frac{\delta V}{\delta \psi} = M \tag{1}$$

Energy Conservation

$$\rho c_p \frac{\delta T}{\delta t} + \frac{\dot{m}\rho c_p}{M}\frac{\delta T}{\delta \psi} = \left(\frac{1}{M}\right)^2 \rho \frac{\delta}{\delta \psi}\left(\lambda \rho A^2 \frac{\delta T}{\delta \psi}\right) - \left(\frac{A}{M}\right)^2 \rho^3 \frac{\delta T}{\delta \psi}\sum_k c_{p,k} D_k \frac{\delta Y_k}{\delta \psi} - \sum_k \dot{\omega}_k \Delta h^0_{f,k} \tag{2}$$

Species Conservation

$$\frac{\delta Y_k}{\delta t} + \frac{\dot{m}}{M}\frac{\delta Y_k}{\delta \psi} = \left(\frac{1}{M}\right)^2 \frac{\delta}{\delta \psi}\left(\rho^2 D_k A^2 \frac{\delta Y_k}{\delta \psi}\right) + \frac{\dot{\omega}_k W_k}{\rho} \tag{3}$$

In Eqns. (1)-(3), V and A are functions of r and the metric factor α depending on the configuration geometry (α = 0 for planar, α = 1 for cylindrical, α = 2 for spherical). These relationships for V and A are given in Eqns. (4) and (5), respectively.

$$V = f(\alpha) r^{\alpha+1} \tag{4}$$

$$A = \frac{\partial V}{\partial r} = f(\alpha)^{1-\beta}(\alpha+1)V^{\beta} \tag{5}$$

where $f(\alpha = 0) = 1$, $f(\alpha = 1) = \pi$, $f(\alpha = 2) = \frac{4}{3}\pi$, and $\beta = {}^{\alpha}/_{(\alpha+1)}$.

B: SLTORC Derivation of S_u^0 and Comparison with Cantera Results

Freely propagating, planar CH_4/air flames with P = 1 atm, and T_u = 300 K varying φ were conducted in SLTORC assuming adiabatic conditions. The FFCM-1 chemical model [2] was used in all CH_4/air planar flame simulations. The flames were allowed to propagate until steady-state was reached, at which the flame propagation speed dx_f/dt reached a constant value such that $dx_f/dt = S_b^0$. In Fig. S1, values for S_u^0 varying φ were derived by multiplying S_b^0 by the density ratio according to Eq. (6).

$$S_u^0 = \left(\frac{\rho_b}{\rho_u}\right) S_b^0 \tag{6}$$

Here, ρ_u is the density of the unburned gas mixture and ρ_b is the density of the burned gas mixture, where ρ_b is approximated as the density of the equilibrated mixture (ρ_{ad}) at T_{ad}. It is important to note that ρ_b is not uniquely defined for flames affected by radiation heat loss, as ρ_b varies along the burned gas and is always greater than ρ_{ad}. However, Eq. (6) is appropriate to use when assuming adiabatic conditions. Derived values for S_u^0 from SLTORC were also compared to S_u^0 computed from steady, planar flames simulated with Cantera at the same unburned gas conditions, shown in Fig. S1. Results for S_u^0 varying φ are shown to agree very well between SLTORC and Cantera, with differences smaller than 0.8% across all cases.

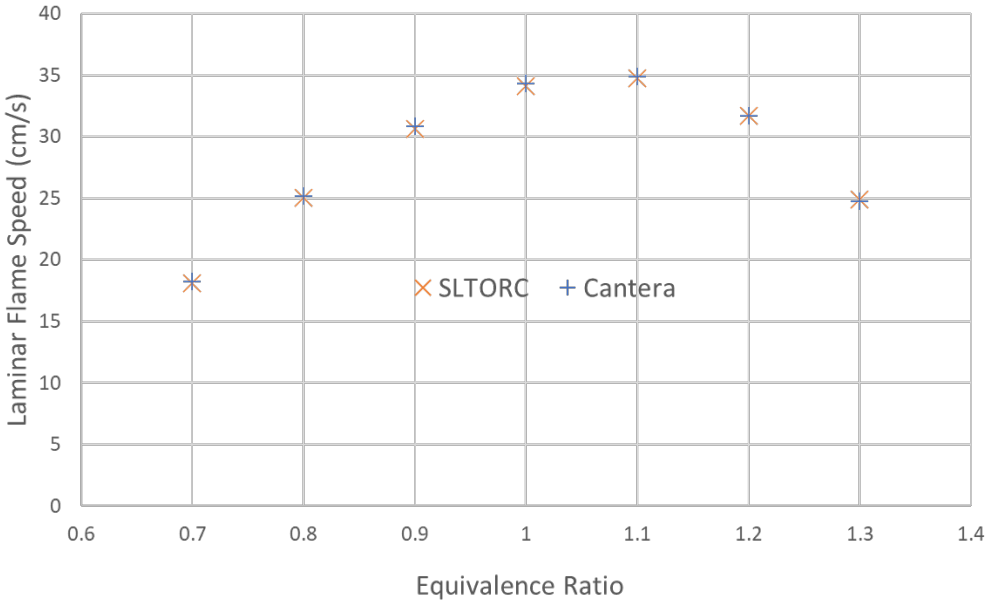

Fig. S1. S_u^0 vs. φ for simulated planar, CH_4/air flames with P = 1 atm and T_u = 300 K. Solid markers indicate the value of φ used in simulations.

C: SLTORC SEF Parameter Descriptions and Solution Convergence

Basilisk and the Adaptive Grid Refinement Algorithm

Adaptive grid refinement in SLTORC is performed through a wavelet-estimated discretization error method within the finite-volume partial-differential-equation solver Basilisk [3]. This adaptive wavelet algorithm ("Adapt Wavelet") is based around the estimation of numerical errors in the representation of spatially-discretized fields [4]. The algorithm first requires a list of variables to analyze for grid refinement/coarsening. The variables used in adaptive grid refinement in SLTORC include temperature (T), the first derivative of temperature (GradT), and the second derivative of temperature (CurveT). The algorithm utilizes a tree-based grid (i.e. a quadtree), whose structure introduces a hierarchy between cells at integer levels of refinement, referred to as the parameter "LEVEL". The solver allows neighboring cells to vary up to one level, where grid resolution differs by a factor of two between levels of refinement. Additionally, the maximum tolerated error, referred to as the parameter "TError," is defined for each input variable. Finally, a maximum level parameter controls the upper limit for grid refinement, referred to as "MaxLEVEL." For a sufficiently defined value for TError (TError < 0.1), MaxLEVEL becomes the major controlling parameter for specifying grid refinement. The use of these parameters in the test case described below can be found in Table S2. A more detailed description of the quadtree-adaptive multigrid solver is provided by Popinet [3], and a more detailed description of the wavelet-estimated discretization error method is provided by Van Hooft et al. [4].

Ignition Kernal Initialization and Flame Radius Tracking

The ignition energy for SLTORC simulations was controlled primarily through the parameters "ignitionMassFraction" or IMF and "Texcess" or T_{ex}. IMF is the fraction of the domain mass used for the burned gas kernel, while T_{ex} is the temperature added to the equilibrated kernel temperature (i.e., $T_b = T_{ad} + T_{ex}$). In addition, specifying the size of the initial kernel through IMF is inherently dependent on the initial size of the domain through the parameter "domainLength" or L_d. The chosen domain geometry, specified with the parameter "metricFac" (i.e., α described above) determines how grid points of equal mass (i.e., material particles in the Lagrangian formulation) are initially distributed along the domain. For SEFs, the burned gas kernel radius ($R_{f,0}$) and deposited ignition energy (E_{ign}) are related to IMF, L_d, and T_b through Eqns. (7) and (8), respectively.

$$R_{f,0} = R_{f,0}(IMF, L_d, T_b) = L_d \sqrt[3]{\frac{(IMF)\bar{M}_{w,u}T_b}{\bar{M}_{w,b}T_u}} \tag{7}$$

$$E_{ign} = E_{ign}(R_{f,0}, T_b) = \frac{4}{3}\pi R_{f,0}^3 \rho_b \int_{T_u}^{T_b} \frac{c_p}{\bar{M}_w} dT \approx \frac{4}{3}\pi R_{f,0}^3 \rho_b \left(\frac{c_{p,b} T_b}{\bar{M}_{w,b}} - \frac{c_{p,u} T_u}{\bar{M}_{w,u}} \right) \quad (8)$$

In Eqns. (6) and (7), $\bar{M}_{w,u}$ and $\bar{M}_{w,b}$ are the mean molecular weights of the unburned and burned gas, respectively. For a specified value for L_d, IMF was varied until the minimum $R_{f,0}$ for successful ignition of an adiabatic flame was determined, holding T_{ex} at 0 K. Afterwards, T_{ex} was increased for the corresponding radiative flame case until successful ignition was achieved for the specified IMF and L_d.

The evolution of the flame radius is tracked using a user-specified "isotherm" or T_{iso}. A consistent value for the isotherm parameter was chosen after considering the relatively low burned gas temperatures at large R_f in weakly propagating HFC/air flames due to significant radiative cooling. For example, the maximum flame temperature of a radiative R-1234yf/air SEF with φ =1.2, P = 1 atm, and T_u = 400 K is approx. 1700 K. At R_f = 3 cm, the temperature at the core of the burned gas had cooled to approx. 1300 K, and at R_f = 6 cm the burned gas core temperature had cooled to approx. 1000 K. To prevent issues with R_f tracking arising from significant radiative cooling in the burned gas, a temperature of 600 K was chosen for the isotherm parameter. Solution convergence tests varying the isotherm parameter were performed for R-32/air SEFs with φ =1.2, P = 1 atm, and T_u = 300 K assuming adiabatic conditions. As shown in Fig. S2, varying the isotherm parameter between 600-1400K had a negligible effect on the evolution of S_b vs. R_f once quasi-steady propagation was achieved.

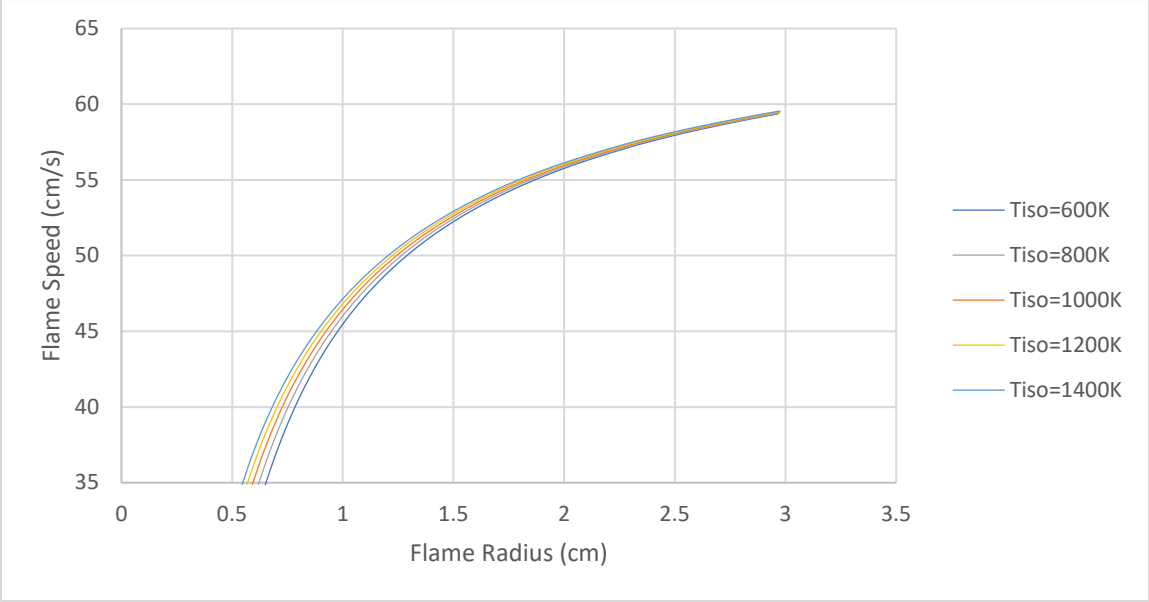

Fig. S2: S_b vs. R_f varying T_{iso} for a spherically expanding R-32/air flame with φ =1.2, P = 1 atm, and T_u = 300 K assuming adiabatic conditions.

Convergence Test Varying Spatial and Temporal Refinement

Solution convergence tests were performed for spherically-expanding R-32/air flames simulated in SLTORC, varying the major spatial refinement criteria (MaxLEVEL) and temporal refinement criteria (dt). Results for a sample solution convergence test are provided below in Figs. S3-S4.

Test Case:

- R-32/air Spherical Flame
- Adiabatic
- φ = 1.2, P = 1 atm, T_u = 300 K

Table S2. Selected SLTORC Input Parameters.

Parameter	Value	Description
pAmbient	1.0	Ambient pressure <atm>
TAmbient	300.0	Unburned gas temperature <K>
comp	CH2F2:1.2, O2:1.0, N2:3.76	Mole fractions of unburned gas species
TExcess	0.0	Excess temperature <K> added to adiabatic flame temperature of initial burned gas kernel
ignitionMassFraction	5.0e-4	Fraction of domain mass equilibrated for initial burned gas kernel
ignitionFlameThickness	0.05	Fraction of domain mass used for hyperbolic tangent region between burned and unburned gas
radiation	false	Switch for turning OTL radiation calculation on/off
domainLength	0.02	Length of domain <m>
metricFac	2	Metric Factor (0 for planar, 1 for cylindrical, 2 for spherical)
maxLEVEL	12, 13, 14, 15, 16	Maximum allowable Level for adaptive grid refinement
TError	0.1	Maximum error criterion for adaptive grid
dt	5e-7, 1e-6, 2e-6, 4e-6	Time step size <s>
isotherm	600.0	Isotherm temperature for tracking R_f <K>

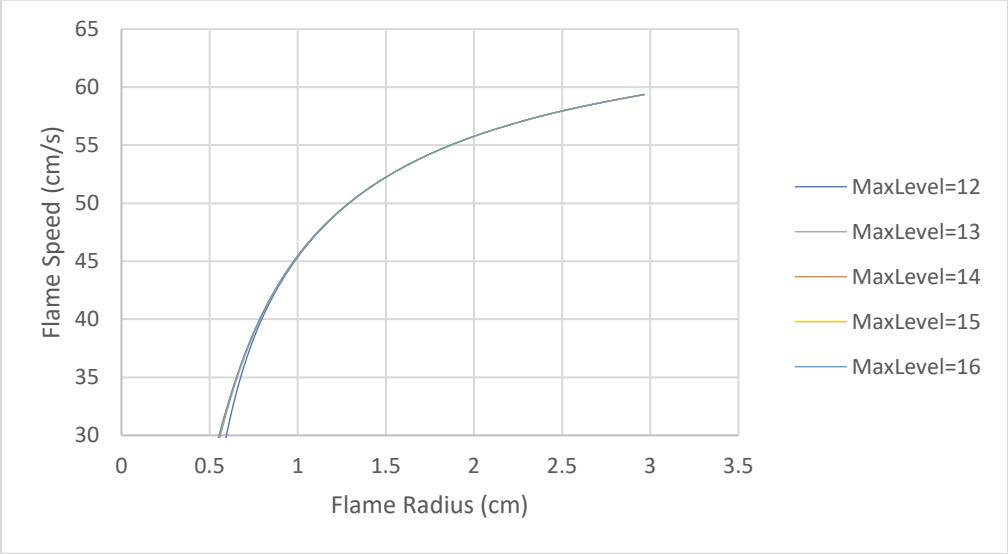

Fig. S3: S_b vs. R_f varying MaxLevel for a spherically expanding R-32/air flame with φ =1.2, P = 1 atm, and T_u = 300 K assuming adiabatic conditions. A consistent value of dt = 1e^{-6} was used in each case.

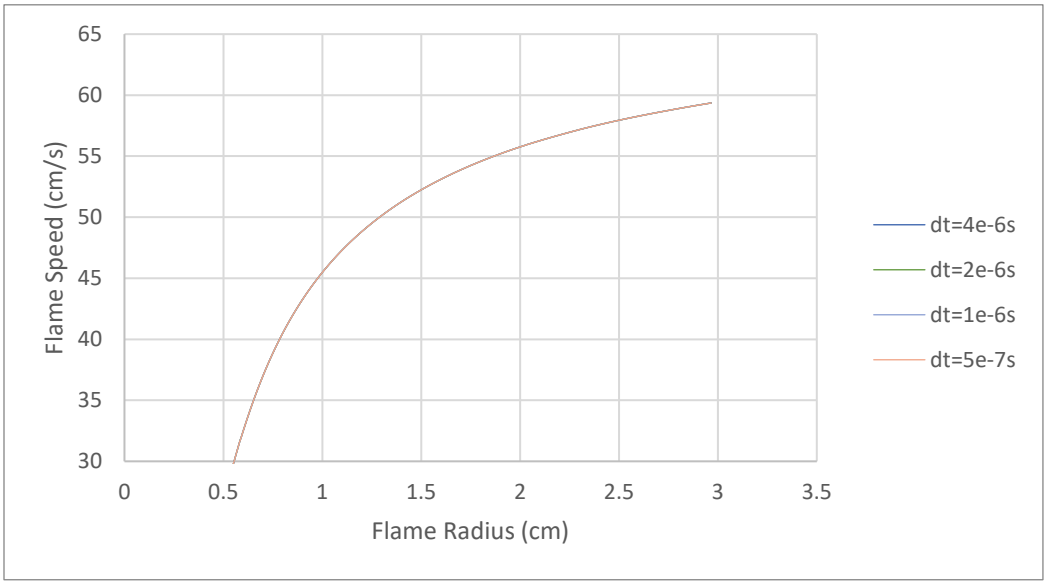

Fig. S4. S_b vs. R_f varying dt for a spherically expanding R-32/air flame with φ =1.2, P = 1 atm, and T_u = 300 K assuming adiabatic conditions. A consistent value of MaxLevel = 15 was used in each case.

D: Deriving S_b^0 Through Zero-stretch Flame Speed Extrapolation

A linear extrapolation to $K = 0$ was performed on the adiabatic dR_f/dt, Santner-corrected S_b, and SRADIF-correced S_b curves for the DNS test case described in Supplementary Material C, shown in Fig. S5. Best least-squared fit parameters for the linear extrapolations are also provided, where the y-intercept of each best fit equation corresponds to S_b^0. The S_b^0 value obtained from extrapolating the adiabatic curve is S_b^0 = 67.83 cm/s, which agrees well with the steady-state value of S_b^0 = 67.66 cm/s for a planar R-32/air flame with equivalent unburned gas conditions, shown in Fig. S6. The steady state value for S_b^0 for the radiative case was derived from an inverted, planar DNS case, which resulted with a steady state value of S_u^0 = 7.02 cm/s, as shown in Fig. S7. The inverted, planar case differs from a normal case in that it is initiated by igniting a burned gas kernel from the right boundary instead of the left, allowing the planar flame to propagate to the left with a negative flame speed into a quiescent unburned gas. This allowed the steady-state flame propagation speed (e.g., S_u^0) to be unaffected by burned gas contraction due to radiative cooling. The steady-state value of S_u^0 can be multiplied by the density ratio (ρ_u/ρ_b) to give a steady-state value of S_b^0 = 61.66 cm/s, which agrees well with the extrapolated value of the SRADIF-corrected S_b curve, which is S_b^0 = 62.838 cm/s as shown in Fig. S5. As previously mentioned, ρ_b is not uniquely defined for flames affected by radiation heat loss and using $\rho_b = \rho_{ad}$ in the density ratio is an approximation.

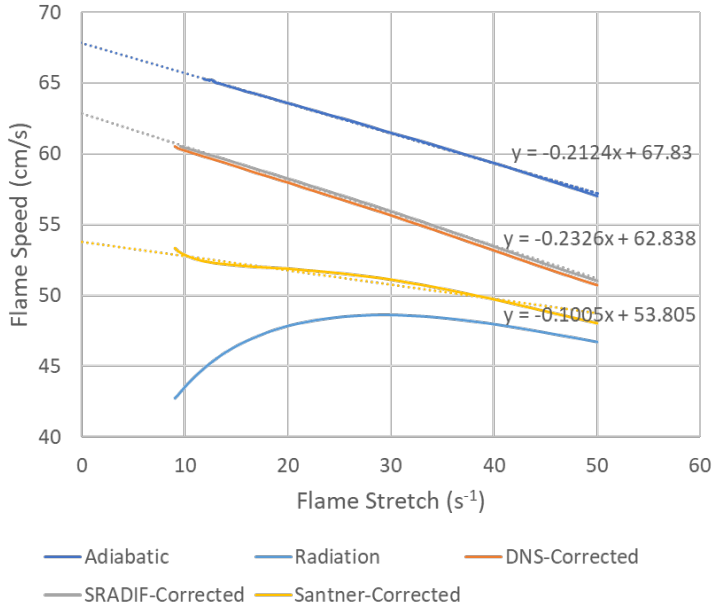

Fig. S5. dR_f/dt and radiation-corrected S_b vs. K for a spherically expanding R-32/air flame with φ =1.2, P = 1 atm, and T_u = 300 K. "Adiabatic" refers to the S_b curve derived from DNS with radiation heat loss neglected. "Radiation" refers to the dR_f/dt curve derived from DNS with radiation heat loss included. "DNS-Corrected" refers to the S_b curve, in which u_b was derived

from DNS results using Eq. (12). "Santner-Corrected" refers to the S_b curve, in which u_b was derived from the analytical model of Santner et al. [5]. "SRADIF-corrected" refers to the S_b curve, in which u_b was derived from the developed SEF radiation model.

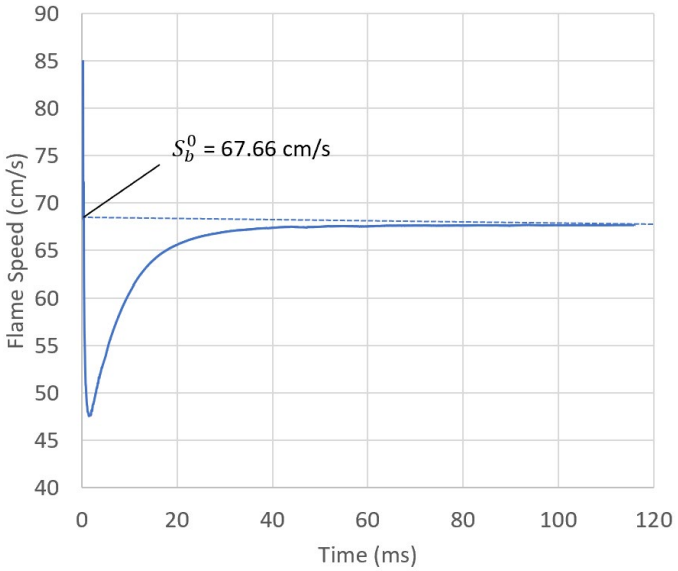

Fig. S6. dR_f/dt vs. t for a planar R-32/air flame with φ =1.2, P = 1 atm, and T_u = 300 K assuming adiabatic conditions.

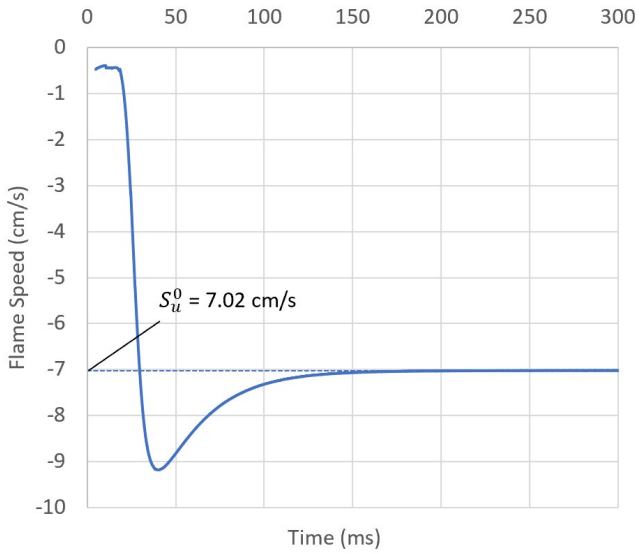

Fig. S7. dR_f/dt vs. t for an inverted, planar R-32/air flame with φ =1.2, P = 1 atm, and T_u = 300 K assuming radiation heat loss.

E: Interpreting Experimental Data Using SRADIF and Comparison to DNS Results

CON-P SEF experimental measurements for R_f vs. t were obtained from Hegetschweiler & coworkers [6,7], who used spherical flame edge and flame curvature methods to process flame images. Measurements for R_f vs. t, derived through the spherical flame curvature method, for a R-32/air flame with initial φ = 1.2, P = 1 atm, and T_u = 300K were used as inputs to the SRADIF model to demonstrate the model's ability to interpret experimental data. The experimental dR_f/dt, SRADIF-derived u_b, and radiation-corrected S_b for this case are compared against DNS results in Figure S8a-b. As the experimental dR_f/dt approaches and coincides with the quasi-steady region of dR_f/dt from DNS, the respective SRADIF-derived u_b and radiation-corrected S_b agree very well for a majority of the relevant range of flame radii. These results highlight SRADIF's ability to interpret experimental measurements, effectively quantifying radiation-induced flow effects in spherical R-32/air flames.

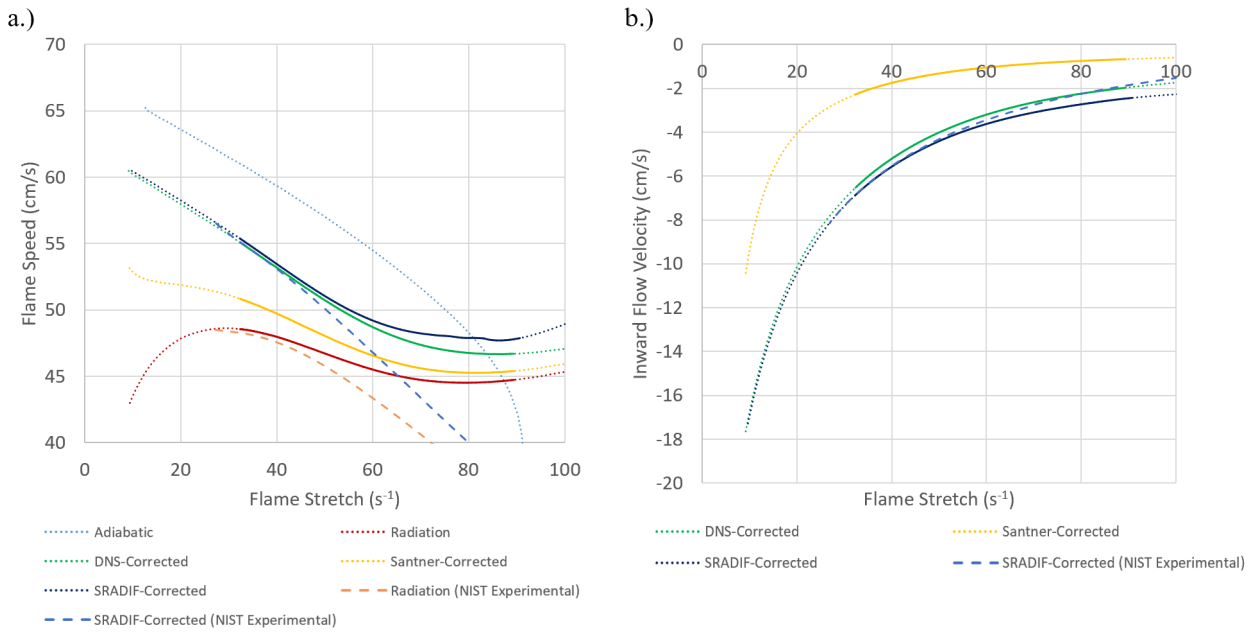

Fig. S8. Spherical, R-32/air flame with φ =1.2, P = 1 atm, and T_u = 300 K. a.) DNS-corrected burned flame speed vs. stretch, b.) Radiation-induced inward flow velocity vs. stretch. Solid region indicates flame radius range applicable to typical CON-P SEF experimental setups (1.0 cm < R_f < 3.0 cm).

F: Derivation for $u_{rad}(r)$ Equation

Table S4. Variable nomenclature for derivation of $u_{rad}(r)$.

r	Radial distance
t	Time
T	Temperature
ρ	Density
P	Pressure
c_p	Specific heat at constant pressure
R	Specific gas constant
u_{rad}	Gas flow velocity induced by radiation heat loss
$\dot{q}_{rad}$	Volumetric radiation heat loss flux
$\dot{q}_{cond}$	Volumetric conduction heat flux
$\dot{q}_{diff}$	Volumetric mass diffusion heat flux
$\dot{q}_{HRR}$	Volumetric chemical heat release flux

Without Convection Term in Energy Equation

Assumptions:

- $P \approx$ constant for all r and t
- $R \approx$ constant for all r and t (within the burned gas region)
- Heat transfer due to conduction, convection, mass diffusion, and chemical heat production/consumption do not affect u_{rad}

Governing Reacting Flow Equations in Spherical Coordinates: [8]

Continuity Equation:

$$\left(\frac{\partial \rho}{\partial t}\right)_{rad} + \frac{1}{r^2}\frac{\partial(\rho u_{rad} r^2)}{\partial r} = 0 \tag{9}$$

Conservation of Energy Equation:

$$\rho c_p \left(\frac{\partial T}{\partial t}\right)_{rad} = -\dot{q}_{rad} \tag{10}$$

Equation of State:

$$P = \rho RT \tag{11}$$

1. Take partial derivatives of the equation of state (Eq. (11)) with respect to t to obtain relationship between derivatives of T and ρ:

$$\left(\frac{\partial T}{\partial t}\right)_{rad} = -\frac{T}{\rho}\left(\frac{\partial \rho}{\partial t}\right)_{rad} \tag{12}$$

2. Substitute $\left(\frac{\partial T}{\partial t}\right)_{rad}$ in conservation of energy equation (Eq. (10)) with Eq. (12):

$$-c_p T\left(\frac{\partial \rho}{\partial t}\right)_{rad} = -\dot{q}_{rad} \tag{13}$$

3. Substitute $\left(\frac{\partial \rho}{\partial t}\right)_{rad}$ from continuity equation (Eq. (9)) into Eq. (13) and simplify:

$$-c_p T\left[-\frac{1}{r^2}\frac{\partial(\rho u_{rad} r^2)}{\partial r}\right] = -\dot{q}_{rad}$$

$$\frac{\partial(\rho u_{rad} r^2)}{\partial r} = -\frac{r^2}{c_p T}\dot{q}_{rad} \tag{14}$$

4. Integrate Eq. (14) with respect to r and simplify to obtain final equation for $u_{rad}(r)$:

$$\partial(\rho u_{rad} r^2) = -\frac{r^2}{c_p T}\dot{q}_{rad}\partial r$$

$$u_{rad}(r) = -\frac{1}{\rho r^2}\int_0^r \frac{\dot{q}_{rad}}{c_p T}\bar{r}^2 \partial \bar{r} \tag{15}$$

Including Convection Term in Energy Equation

Assumptions:

- $P \approx$ constant for all r and t
- $R \approx$ constant for all r and t (within the burned gas region)
- Heat transfer due to conduction, mass diffusion, and chemical heat production/consumption do not affect u_{rad}
- Convective heat transfer affects u_{rad} by accounting for burned gas shrinkage and its effect on the unburned gas flow

Governing Reacting Flow Equations in Spherical Coordinates: [8]

Continuity Equation:

$$\left(\frac{\partial \rho}{\partial t}\right)_{rad} + \frac{1}{r^2}\frac{\partial(\rho u_{rad} r^2)}{\partial r} = 0 \tag{16}$$

Conservation of Energy Equation:

$$\rho c_p \left(\frac{\partial T}{\partial t}\right)_{rad} + \rho u_{rad} c_p \frac{\partial T}{\partial r} = -\dot{q}_{rad} \tag{17}$$

Equation of State:

$$P = \rho R T \tag{18}$$

1. Take partial derivatives of the equation of state (Eq. (18)) with respect to t and r to obtain relationship between partial derivatives of T and ρ:

$$\left(\frac{\partial T}{\partial t}\right)_{rad} = -\frac{T}{\rho}\left(\frac{\partial \rho}{\partial t}\right)_{rad} \tag{19}$$

$$\frac{\partial T}{\partial r} = -\frac{T}{\rho}\frac{\partial \rho}{\partial r} \tag{20}$$

2. Substitute $\left(\frac{\partial T}{\partial t}\right)_{rad}$ and $\frac{\partial T}{\partial r}$ in conservation of energy equation (Eq. (17)) with Eq. (19) and Eq. (20), respectively:

$$-c_p T\left(\frac{\partial \rho}{\partial t}\right)_{rad} - u_{rad} c_p T\frac{\partial \rho}{\partial r} = -\dot{q}_{rad} \tag{21}$$

3. Substitute $\left(\frac{\partial \rho}{\partial t}\right)_{rad}$ from continuity equation (Eq. (16)) into Eq. (21) and simplify:

$$-c_p T\left[-\frac{1}{r^2}\frac{\partial(\rho u_{rad} r^2)}{\partial r}\right] - u_{rad} c_p T\frac{\partial \rho}{\partial r} = -\dot{q}_{rad}$$

$$\frac{\partial(\rho u_{rad} r^2)}{\partial r} - u_{rad} r^2\frac{\partial \rho}{\partial r} = -\frac{r^2}{c_p T}\dot{q}_{rad} \tag{22}$$

4. Perform product rule expansion for first LHS term of Eq. (22):

$$\frac{\partial(\rho u_{rad} r^2)}{\partial r} = u_{rad} r^2\frac{\partial \rho}{\partial r} + \rho\frac{\partial(u_{rad} r^2)}{\partial r} \tag{23}$$

5. Substitute Eq. (23) into Eq. (22) and cancel like terms:

$$u_{rad} r^2 \frac{\partial \rho}{\partial r} + \rho \frac{\partial (u_{rad} r^2)}{\partial r} - u_{rad} r^2 \frac{\partial \rho}{\partial r} = -\frac{r^2}{c_p T} \dot{q}_{rad}$$

$$\rho \frac{\partial (u_{rad} r^2)}{\partial r} = -\frac{r^2}{c_p T} \dot{q}_{rad} \tag{24}$$

6. Integrate Eq. (24) with respect to r and simplify to obtain final equation for $u_{rad}(r)$:

$$\partial (u_{rad} r^2) = -\frac{r^2}{\rho c_p T} \dot{q}_{rad} \partial r$$

$$u_{rad}(r) = -\frac{1}{r^2} \int_0^r \frac{\dot{q}_{rad}}{\rho c_p T} \bar{r}^2 \partial \bar{r} \tag{25}$$

Including All Terms in Energy Equation

- $P \approx$ constant for all r and t
- $R \approx$ constant for all r and t (within the burned gas region)

Governing Reacting Flow Equations in Spherical Coordinates: [8]

Continuity Equation:

$$\frac{\partial \rho}{\partial t} + \frac{1}{r^2} \frac{\partial (\rho u r^2)}{\partial r} = 0 \tag{26}$$

Conservation of Energy Equation:

$$\rho c_p \frac{\partial T}{\partial t} + \rho u c_p \frac{\partial T}{\partial r} = \dot{q}_{cond} + \dot{q}_{diff} + \dot{q}_{HRR} - \dot{q}_{rad} \tag{27}$$

$$\rho c_p \frac{\partial T}{\partial t} + \rho u c_p \frac{\partial T}{\partial r} = \frac{1}{r^2}\frac{\partial}{\partial r}\left(\lambda r^2 \frac{\partial T}{\partial r}\right) + \rho \frac{\partial T}{\partial r}\sum_k c_{p,k} D_k \frac{\partial Y_k}{\partial r} + \sum_k \dot{\omega}_k \Delta h_{f,k}^0 - \dot{q}_{rad} \quad (28)$$

Equation of State:

$$P = \rho R T \quad (29)$$

1. Following a similar procedure used to derive Eqns. (19)-(25), an equation for estimating the total gas velocity $u(r)$ within the burned gas ($0 < r < \min(u_{rad}(r))$ considering contributions from all heat terms of the conservation of energy equation is derived:

$$u(r) = -\frac{1}{r^2}\int_0^r \frac{\bar{r}^2}{\rho c_p T}\left[\dot{q}_{cond} + \dot{q}_{diff} + \dot{q}_{HRR} - \dot{q}_{rad}\right]\partial \bar{r} \quad (30)$$

G: R-1234yf Chemical Mechanism DRG Reduction

The direct relation graph (DRG) method [9] was used to reduce the R-1234yf chemical model obtained from NIST (hfc-yf-zee-zf-model-b.cti) [10]. This chemical model is published in NIST's technical note, which includes the exact mechanism in text form. The DRG method was performed using pyMARS. Adiabatic flame solutions for equivalence ratios (φ) of 0.8-1.2 at P =1 atm and T_u = 400 K were utilized. Under these conditions, the chemical model was reduced from 113 species and 1064 reactions to 50 species and 269 reactions. The reduced chemical model (named reduced_50_hfc_r1234yf_sep32021.cti) was used in all planar freely propagating flame simulations (Cantera) and spherically expanding flame simulations (SLTORC) to reduce computational costs. The reduced_50_hfc_r1234yf_sep32021.cti chemical model file, as well as the chemical kinetic, thermodynamic, and transport files, have been included as supplementary material.

To further validate the applicability of the reduced chemical model to conditions near those used in the DRG chemical model reduction, planar freely propagating R-1234yf/air flame simulations were performed in Cantera for a range of equivalence ratios at P = 1 atm and T_u = 300 K using both the full and reduced chemical models for R-1234yf. These results are shown in Fig. S9. Although the unburned temperature of 300 K, as well as equivalence ratios of 0.7 and 1.3, were not included as conditions in the DRG chemical model reduction, the reduced chemical model still produces accurate results for the laminar flame speed, with a maximum deviation of 3.19% between the full and reduced chemical models.

In addition, the reduced chemical model appears to have slightly increased the reactivity (higher laminar flame speeds) for these R-1234/air flames. This supports the prediction that the chemical model reduction did not reduce the flammability of radiative R-1234yf/air flames at T_u = 300 K, which were interpreted to be "non-flammable" as a result of numerical convergence errors.

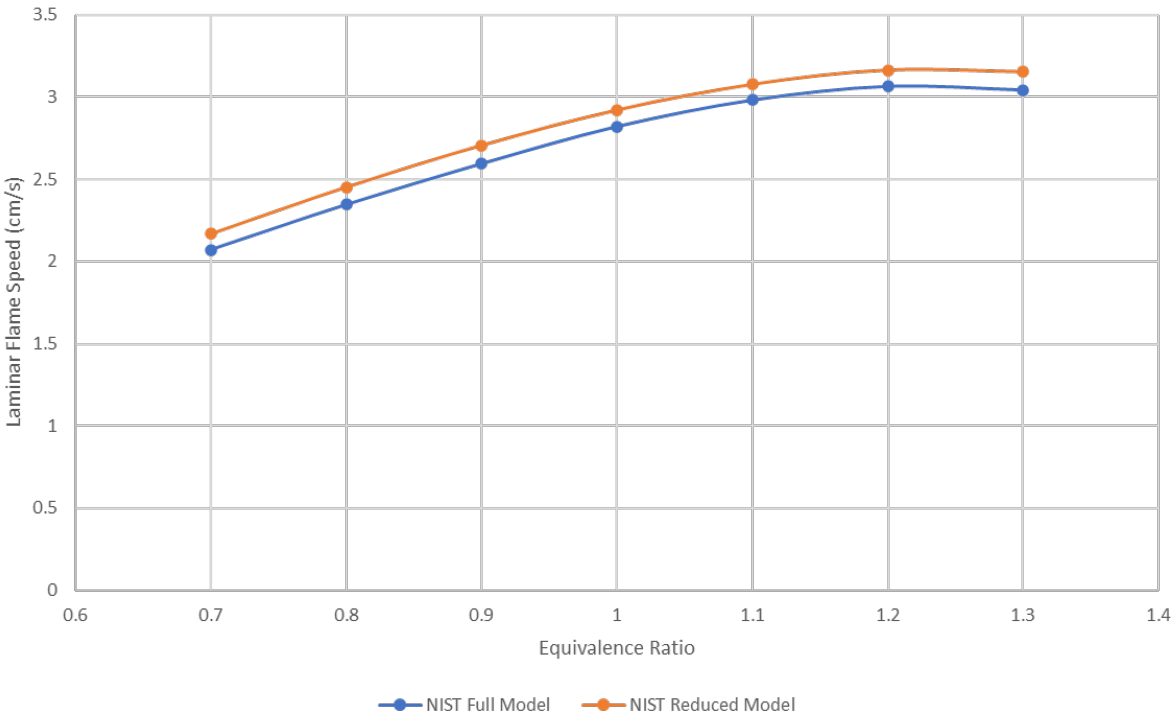

Fig. S9. Planar, R-1234yf/air flame with P = 1 atm, and T_u = 300 K varying equivalence ratio (φ) assuming adiabatic conditions.

References

[1] R. Lawson, V. Gururajan, A. Movaghar, F.N. Egolfopoulos, Autoignition of reacting mixtures at engine-relevant conditions using confined spherically expanding flames, Proc. Combust. Inst. 38 (2021) 2285-2293.

[2] G.P. Smith, Y. Tao, and H. Wang, Foundational Fuel Chemistry Model Version 1.0 (FFCM-1), http://nanoenergy.stanford.edu/ffcm1, 2016.

[3] S. Popinet, A quadtree-adaptive multigrid solver for the Serre–Green–Naghdi equations, J. Comput. Phys. 302 (2015) 336-358.

[4] J.A. van Hooft, S. Popinet, C.C. van Heerwaarden, S.J.A. van der Linden, S.R. de Roode, B.J.H. van de Wiel, Towards adaptive grids for atmospheric boundary-layer simulations, Bound.-Layer Meteorol. 167 (2018) 421-443.

[5] J. Santner, F.M. Haas, Y. Ju, F.L. Dryer, Uncertainties in interpretation of high pressure spherical flame propagation rates due to thermal radiation, Combust. Flame 161 (2014) 147-153.

[6] M.J. Hegetschweiler, J.L. Pagliaro, L. Berger, R. Hesse, J. Beeckmann, C. Bariki, H. Pitsch, G.T. Linteris, Data reduction considerations for spherical R-32(CH2F2)-air flame experiments, Combust. Flame 237 (2022) 111806.

[7] G. Linteris, personal communication, 2023.

[8] D. Bradley, P.H. Gaskell, X.J. Gu, Burning velocities, Markstein lengths, and flame quenching for spherical methane-air flames: A computational study, Combust. Flame 104(1-2) (1996) 176-198.

[9] T. Lu, C.K. Law, A directed relation graph method for mechanism reduction, Proc. Combust. Inst. 30 (2005) 1333–1341

[10] V.I. Babushok, D.R. Burgess Jr, D.K. Kim, M.J. Hegetschweiler, G.T. Linteris, Modeling of Combustion of Fluorine-Containing Refrigerants, NIST Technical Note TN 2170 (2021).